PHYSICAL REVIEW A **79**, 043624 (2009)

Directional effects due to quantum statistics in dissociation of elongated molecular condensates

Magnus Ögren,[1] C. M. Savage,[2] and K. V. Kheruntsyan[1]
[1]*ARC Centre of Excellence for Quantum-Atom Optics, School of Physical Sciences, University of Queensland, Brisbane, QLD 4072, Australia*
[2]*Department of Quantum Science, ARC Centre of Excellence for Quantum-Atom Optics, Australian National University, Canberra, ACT 0200, Australia*
(Received 22 September 2008; published 23 April 2009)

Ultracold clouds of dimeric molecules can dissociate into quantum mechanically correlated constituent atoms that are either both bosons or both fermions. We theoretically model the dissociation of two-dimensional anisotropic molecular condensates for which this difference manifests as complementary geometric structures of the dissociated atoms. Atomic bosons are preferentially emitted along the long axis of the molecular condensate, while atomic fermions are preferentially emitted along the short axis. This anisotropy potentially simplifies the measurement of correlations between the atoms through relative number squeezing.

DOI: 10.1103/PhysRevA.79.043624 PACS number(s): 03.75.−b, 03.65.−w, 05.30.−d, 33.80.Gj

I. INTRODUCTION

The difference between bosons and fermions is fundamental in physics. Ultracold degenerate quantum gases enable new kinds of explorations and applications of this difference. For example in Hanbury, Brown, and Twiss type measurements bosonic ^{4}He atoms are observed to be bunched while fermionic ^{3}He atoms are antibunched [1]. Besides such local spatial correlations, nonlocal correlations between pairs of atoms with opposite momenta have also been observed for both fermionic atoms [2] and bosonic atoms [3]. Such atom pairs, generated by dissociation of molecular dimers [2] or by four-wave mixing [3], are predicted to be entangled [4–11]. However, the existence of nonclassical Einstein-Podolsky-Rosen type correlations [4,8] between atom pairs in these systems remains to be experimentally confirmed.

We report an analysis of the effect of particle statistics on the dissociation of highly anisotropic Bose-Einstein condensates (BECs) of molecular dimers. When the dissociated atoms are bosons we confirm the expected enhanced emission of atoms along the long axis of the cigar-shaped molecular condensate due to stimulated emission [7]. However, when the atoms are fermions we find an unexpected enhancement in the orthogonal direction: that is, along the short condensate axis. The effect is due to Pauli blocking followed by atom-atom recombination which reduces the atomic density along the long axis. We also find strong relative number squeezing between the atoms in the half spaces occupied by the lobes of enhanced atom number.

Directionality effects due to bosonic amplification have been observed [12,13] in super-radiant light scattering from elongated condensates [7,14,15]. The fermionic counterpart of the effect due to Pauli blocking has not been discussed before to the best of our knowledge. Our results provide a particularly dramatic and accessible demonstration of the fundamental difference between bosons and fermions. This difference alone results in enhanced emission in perpendicular directions. Furthermore, the opposite emission lobes show substantial number difference squeezing. This anisotropic distribution of atoms with nonlocal quantum correlations provides a potentially valuable tool for the application and investigation of atomic entanglement in mesoscopic regimes [8].

II. MODEL

In the following we shall only consider two spatial dimensions (2D), with $\mathbf{x}=(x,y)$. This is to make the problem numerically tractable. However, based on the physical understanding that we develop, we expect our results to be at least qualitatively valid for three-dimensional (3D) systems.

The effective quantum-field-theory Hamiltonian describing the system in the undepleted molecular-field approximation and in the absence of two-body s-wave scattering interactions is, in a rotating frame [16]

$$\hat{H}=\hbar\int d\mathbf{x}\Bigg[\sum_{i=1,2}\hbar|\nabla\hat{\Psi}_i|^2/2m + \sum_{i=1,2}\Delta\hat{\Psi}_i^\dagger\hat{\Psi}_i - ig(\mathbf{x})(\hat{\Psi}_1\hat{\Psi}_2-\hat{\Psi}_2^\dagger\hat{\Psi}_1^\dagger)\Bigg]. \quad (1)$$

Here, $\hat{\Psi}_i(\mathbf{x},t)$ $(i=1,2)$ are the field operators for the atoms, which are two different spin states of the same isotope of mass m and may be either bosonic or fermionic. The field operators satisfy the respective commutation or anticommutation relations $[\hat{\Psi}_i(\mathbf{x},t),\hat{\Psi}_j^\dagger(\mathbf{x}',t)]=\delta_{ij}\delta^2(\mathbf{x}-\mathbf{x}')$ and $\{\hat{\Psi}_i(\mathbf{x},t),\hat{\Psi}_j^\dagger(\mathbf{x}',t)\}=\delta_{ij}\delta^2(\mathbf{x}-\mathbf{x}')$. The spatially dependent function $g(\mathbf{x})$ is the effective dissociation strength, which absorbs the molecular mean-field amplitude, as discussed below.

The dissociation detuning Δ is defined so that spontaneous dissociation of molecules corresponds to $\Delta<0$, with $2\hbar|\Delta|$ being the total dissociation energy that is converted into the kinetic energy of atom pairs [17,18]. For molecules at rest, the dissociation primarily populates the resonant atomic modes in the two spin states having equal but opposite momenta, $\hbar\mathbf{k}_1=-\hbar\mathbf{k}_2$, with the absolute wave number equal to $k_0=|\mathbf{k}_1|=|\mathbf{k}_2|=\sqrt{2m|\Delta|/\hbar}$.

The undepleted molecular-field approximation employed in the Hamiltonian Eq. (1) represents the molecular BEC as a

fixed classical field. It is valid for short enough dissociation times that the converted fraction of molecules does not exceed about 10% [17,19]. We have confirmed the validity of this approximation in the case of dissociation into bosonic atoms by comparing the present results to exact, first-principles simulations using the positive-P representation [19] in Sec. III A. For the case of fermionic atoms, first-principles simulations with multimode inhomogeneous molecular condensates remain under development [20] and such a comparison is not presently possible.

We assume that the classical molecular field has the density profile $\rho_M(\mathbf{x})$ given by the ground-state solution of the Gross-Pitaevskii equation in an anisotropic harmonic trap. We then have an effective, spatially dependent dissociation strength

$$g(\mathbf{x}) = \chi\sqrt{\rho_M(\mathbf{x})}, \tag{2}$$

which absorbs the molecular mean-field amplitude $\langle\hat{\Psi}_M(\mathbf{x})\rangle = \sqrt{\rho_M(\mathbf{x})}$, which we assume is real without the loss of generality. The coupling coefficient χ [17] is responsible for coherent conversion of molecules into atom pairs, e.g., via optical Raman transitions, an rf pulse, or a Feshbach resonance sweep [21–25]. We assume that once the dissociation is switched on at time $t=0$, the trapping potential is switched off, so that the evolution is taking place in free space. Thus the role of the trapping potential is reduced to defining the initial shape of the molecular BEC.

In the undepleted molecular-field approximation, the dissociation typically produces low-density atomic clouds for which the atom-atom s-wave scattering interactions are negligible [19]; hence their absence from our Hamiltonian. Additionally, the atom-molecule interaction in this approximation would appear as an effective spatially dependent detuning that can be neglected provided it is much smaller than the magnitude of the dissociation detuning $|\Delta|$. S-wave scattering lengths are tunable around Feshbach resonances. In the following we assume that the atom-molecule interaction is negligible too; for $|\Delta|=281\ \mathrm{s}^{-1}$ and other parameter values that we employ below, this would require an atom-molecule scattering length of $\lesssim 0.1$ nm (see also Ref. [26]). When this approximation is not valid the detailed behavior will be different. However, the physical mechanisms we identify in Sec. III A will remain valid.

The Heisenberg equations for the atomic fields in the Hamiltonian (1) are then

$$\frac{\partial\hat{\Psi}_1(\mathbf{x},t)}{\partial t} = i\left[\frac{\hbar}{2m}\nabla^2 - \Delta\right]\hat{\Psi}_1(\mathbf{x},t) \pm g(\mathbf{x})\hat{\Psi}_2^\dagger(\mathbf{x},t),$$

$$\frac{\partial\hat{\Psi}_2^\dagger(\mathbf{x},t)}{\partial t} = -i\left[\frac{\hbar}{2m}\nabla^2 - \Delta\right]\hat{\Psi}_2^\dagger(\mathbf{x},t) + g(\mathbf{x})\hat{\Psi}_1(\mathbf{x},t). \tag{3}$$

The + (−) in the first equation corresponds to bosonic (fermionic) atoms.

Expanding in plane-wave modes, $\hat{\Psi}_j(\mathbf{x},t) = \int d^2\mathbf{k}\hat{a}_j(\mathbf{k},t)\exp(-i\mathbf{k}\cdot\mathbf{x})/2\pi$, where the operator amplitudes satisfy commutation or anticommutation relations, $[\hat{a}_i(\mathbf{k},t),\hat{a}_j^\dagger(\mathbf{k}',t)] = \delta_{ij}\delta^2(\mathbf{k}-\mathbf{k}')$ or $\{\hat{a}_i(\mathbf{k},t),\hat{a}_j^\dagger(\mathbf{k}',t)\} = \delta_{ij}\delta^2(\mathbf{k}-\mathbf{k}')$, according to the underlying statistics. The partial differential equations (3) reduce to a set of linear ordinary differential equations,

$$\frac{d\hat{a}_1(\mathbf{k},t)}{dt} = -i\Delta_k\hat{a}_1(\mathbf{k},t) \pm \int\frac{d^2\mathbf{q}}{2\pi}\tilde{g}(\mathbf{q}+\mathbf{k})\hat{a}_2^\dagger(\mathbf{q},t),$$

$$\frac{d\hat{a}_2^\dagger(\mathbf{k},t)}{dt} = i\Delta_k\hat{a}_2^\dagger(\mathbf{k},t) + \int\frac{d^2\mathbf{q}}{2\pi}\tilde{g}(\mathbf{q}-\mathbf{k})\hat{a}_1(-\mathbf{q},t), \tag{4}$$

where $\tilde{g}(\mathbf{k}) = \int d^2\mathbf{x}g(\mathbf{x})\exp(i\mathbf{k}\cdot\mathbf{x})/2\pi$ is the Fourier transform of $g(\mathbf{x})$ and $\Delta_k \equiv \hbar k^2/(2m)+\Delta$, where $k=|\mathbf{k}|$. For vacuum initial conditions the nonzero second-order moments in this system are the normal and anomalous densities, $n_i(\mathbf{k},\mathbf{k}',t) \equiv \langle\hat{a}_i^\dagger(\mathbf{k},t)\hat{a}_i(\mathbf{k}',t)\rangle$ and $m_{12}(\mathbf{k},\mathbf{k}',t) \equiv \langle\hat{a}_1(\mathbf{k},t)\hat{a}_2(\mathbf{k}',t)\rangle$. Higher-order moments can be obtained from these second-order moments using Wick's theorem, as the Hamiltonian is quadratic in the field operators in the undepleted molecular approximation.

III. RESULTS AND DISCUSSION

A. Atomic density distributions in momentum space

In a finite quantization volume the wave vector $\mathbf{k}$ is discrete and the plane-wave mode annihilation and creation operators may be organized into a vector $\vec{\hat{a}}$. The Heisenberg equations (4) may then be written in vector-matrix form as $d\vec{\hat{a}}/dt = M\vec{\hat{a}}$, where M is a square matrix of complex numbers of dimension equal to twice the total number of lattice points. The solutions of these operator equations can be found by numerically computing the matrix exponential $\exp(Mt)$. We used an 81×81 numerical lattice in momentum space, which gave the same results as for a 61×61 lattice.

Here we explore the role of a strongly anisotropic system by assuming that the initial molecular condensate was trapped in a harmonic potential with a frequency along the y axis, ω_y, that is 10 times that along the x axis, ω_x, $\omega_y = 10\omega_x$. Although we ignore atom-atom and atom-molecule interactions, for convenience we assume a molecule-molecule scattering length such that the Thomas-Fermi (TF) approximation is valid. The corresponding molecular density profile is $\rho_M = \max\{\rho_{M,0}(1-x^2/R_{\mathrm{TF},x}^2 - y^2/R_{\mathrm{TF},y}^2), 0\}$, where the $R_{\mathrm{TF},i}$ are the TF radii in each direction. The parameter values we used are as follows: molecular BEC peak density $\rho_{M,0}=3.2\times 10^{13}\ \mathrm{m}^{-2}$, number of molecules $N_M = 2\times 10^4$, atomic mass $m = 6.5\times 10^{-26}$ kg (^{40}K), molecule-atom coupling coefficient $\chi = 7.1\times 10^{-5}\ \mathrm{ms}^{-1}$, and dissociation detuning $\Delta = -281\ \mathrm{s}^{-1}$, which is large enough to ensure that the dissociation energy is larger than thermal at nanokelvin temperatures. The momentum lattice had a spacing $\Delta k_x = \Delta k_y = 3.0\times 10^4\ \mathrm{m}^{-1}$, which is smaller than the smallest width of the molecular momentum distribution. Our numerical grid is chosen to resolve relevant structures in both real space and in momentum space.

Figure 1 shows the density of our initial 2D molecular condensate in position space and the density of the dissociated atoms in momentum space at three times as dissociation progresses. The left column shows bosonic atoms and the

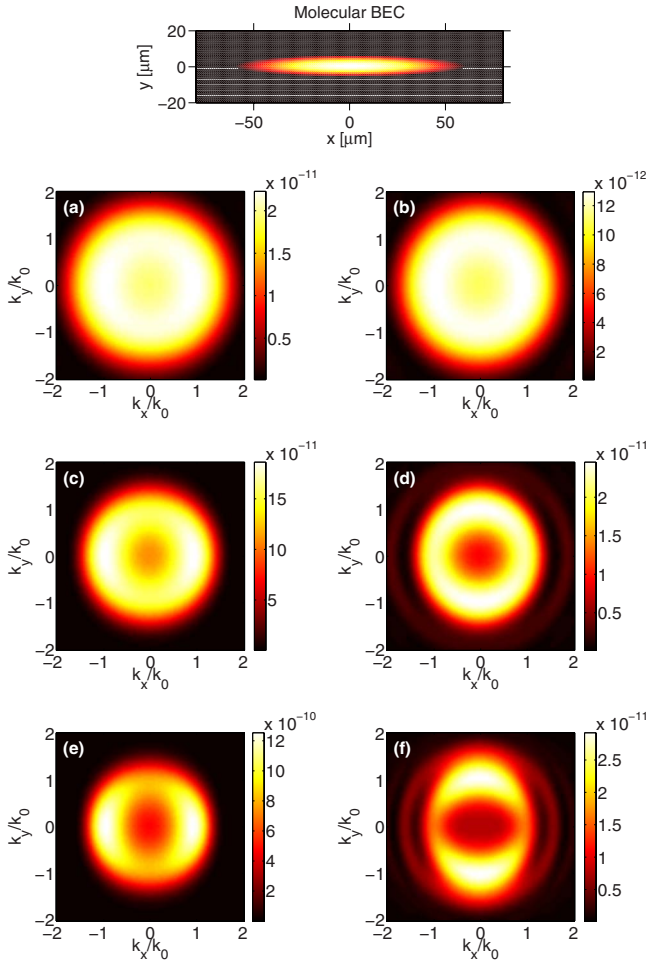

FIG. 1. (Color online) Upper panel: Density in position space for the initial molecular condensate showing the geometry of the system. It corresponds to the ground state of a harmonic trap with TF radii: $R_{\mathrm{TF},x} \simeq 60\ \mu$m and $R_{\mathrm{TF},y} \simeq 6\ \mu$m [27]. (a)–(f) 2D atomic density in momentum space (in units of m^2) at different times t after the start of dissociation. The left and right columns are for bosonic and fermionic atoms, respectively. We have chosen the times $t_1/t_0 = 1.1$ for (a) and (b), $t_2/t_0 = 2.2$ for (c) and (d), and $t_3/t_0 = 3.3$ for (e) and (f), with $t_0 = 1/(\chi\sqrt{\rho_{M,0}}) = 2.5$ ms being the time scale.

right column shows fermionic atoms. Note that after sufficient time-of-flight expansion, these momentum space distributions are reproduced in position space [2,10]. At the earliest time there is little difference between the bosons and fermions and the width of the distribution is determined by the energy-time uncertainty relation. Later, the spatial distributions of the bosons and fermions develop quite differently.

The highest densities of bosons develop along the long axis of the molecular condensate. In contrast, the highest densities of fermions occur in the orthogonal direction, that is, along the short axis of the initial molecular condensate. Physically, the effect in the bosonic case is due to Bose stimulation, which in the undepleted molecular-field approximation leads to approximately exponential growth of the atom number [19]. In the fermionic case, the effect is due to Pauli blocking followed by the reduction of the atomic density due to atom-atom recombination along the long axis. The dynamics along the short axis (for sufficiently small

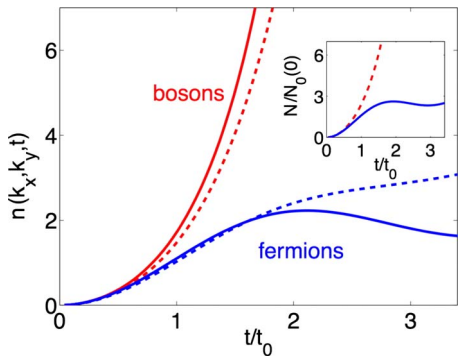

FIG. 2. (Color online) Atomic density in momentum space at the position of resonance ($|\mathbf{k}| = k_0$) along the two different Cartesian directions, in units of 10^{-11} m^2. The two upper (red) curves are for bosons, which grow exponentially due to Bose stimulation. The two lower (blue) curves are for fermions. Solid lines are along the k_x direction ($k_x = k_0, k_y = 0$) and dashed lines are along the k_y direction ($k_x = 0, k_y = k_0$). Inset shows the fractional atom number (relative to the total initial number of molecules), in units of tenths of a percent, for fermions (solid blue) and bosons (dashed red).

$R_{\mathrm{TF},y}$), on the other hand, does not reach the regime dominated by saturation of mode populations and atom-atom recombination as the atoms propagating along the y direction leave the molecular condensate earlier than those propagating along the x direction.

Mathematically, the difference is due to the sign difference on the right-hand side of the Heisenberg equations (3), corresponding to bosons and fermions. As noted in Ref. [28] the sign difference determines $\sinh(\alpha_k t/t_0)$ population growth for bosons and $\sin(\alpha_k t/t_0)$ population oscillations for fermions, where the time scale $t_0 = 1/(\chi\sqrt{\rho_{M,0}})$ and $\alpha_k = \sqrt{1 \pm t_0^2[\hbar k^2/(2m) + \Delta]^2}$; here, the + corresponds to fermions and the − to bosons.

The fermionic oscillations—both in momentum space and in time—can be seen in Figs. 1(d), 1(f), and 2. As the solutions of Ref. [28] are for spatially homogeneous systems they do not quantitatively describe these minima for our inhomogeneous molecular condensate. Nevertheless, they predict aspects of the qualitative behavior, such as the movement of the density minima and maxima to lower values of k_x with increasing time [Figs. 1(d) and 1(f)]. The single density maximum along the k_y axis is a result of the small TF radius along that axis, $R_{\mathrm{TF},y} = 6\ \mu$m. The atomic velocity at $|k/k_0| = 1$ is 0.95 mm s^{-1}, so during $t_1 = 1.1t_0 = 1.1(2.5$ ms) the atoms travel 2.6 μm and during $t_3 = 3.3t_0$ they travel 7.8 μm, which is greater than the TF radius $R_{\mathrm{TF},y}$. Hence a particular atom traveling in the y direction typically interacts with the molecular condensate for less than the time t_3. This accounts for the similarity of Figs. 1(d) and 1(f) along the y axis.

In the case of bosonic atoms, we can compare the results of the present treatment to exact first-principles simulations using the positive-P representation method [10,19]. In the positive-P method the molecular field and its depletion are treated quantum mechanically. Figure 3 shows the atomic density distribution in momentum space obtained from the positive-P simulations for the same parameters as Fig. 1 and

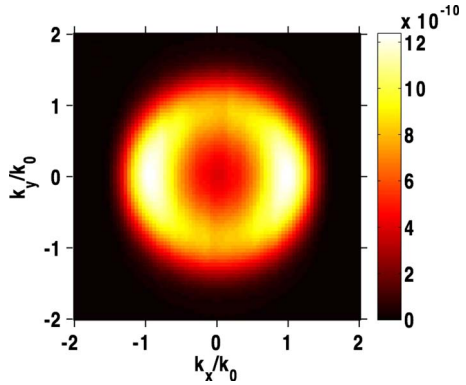

FIG. 3. (Color online) Atomic density distribution in momentum space (in units of m^2) at $t_3/t_0=3.3$ calculated using the positive-P representation. The distribution can be compared to that of Fig. 1(e).

corresponding to time $t/t_0=3.3$. This is the same case as in Fig. 1(e). As we see the agreement between the two results is very good. This result validates both our numerical approach and the undepleted molecular-field approximation. For fermionic atoms, first-principles simulations are under development as previously discussed. However, we expect a similarly good agreement as the molecular depletion is a weaker effect in this case [17,28].

B. Shot noise and relative number squeezing

We have used our solutions of the Heisenberg equations (4) to calculate the correlations between atom number fluctuations in the two different spin states 1 and 2. We considered momentum areas centered on the opposite resonant momenta, $\hbar\mathbf{k}_0$ and $-\hbar\mathbf{k}_0$, for the smallest and largest possible areas in which the atoms are detected and their number measured. The smallest momentum areas are the numerical lattice areas and the largest are opposite halves of the momentum space. These are orientated differently for fermions and bosons, guided by Figs. 1(e) and 1(f): for bosons the halves are split by the k_y axis and for fermions by the k_x axis.

For the case of the smallest momentum area (the area of the numerical lattice cell, $\Delta k_x \Delta k_y$), we define the atom number operators via $\hat{n}_{j,\pm\mathbf{k}_0}(t)=\hat{n}_j(\pm\mathbf{k}_0,t)\Delta k_x\Delta k_y$, where $\mathbf{k}_0=k_0\mathbf{e}_x$ for bosons and $\mathbf{k}_0=k_0\mathbf{e}_y$ for fermions, with $\mathbf{e}_x$ and $\mathbf{e}_y$ being the Cartesian unit vectors. We quantify the correlations by the normalized relative atom number variance,

$$V_{\mathbf{k}_0,-\mathbf{k}_0}(t)=\langle[\Delta(\hat{n}_{1,\mathbf{k}_0}-\hat{n}_{2,-\mathbf{k}_0})]^2\rangle/\Delta_{\mathrm{SN}}, \tag{5}$$

where $\Delta\hat{C}=\hat{C}-\langle\hat{C}\rangle$ is the fluctuation in $\hat{C}$ and $\Delta_{\mathrm{SN}}=\langle(\Delta\hat{n}_{1,\mathbf{k}_0})^2\rangle+\langle(\Delta\hat{n}_{2,-\mathbf{k}_0})^2\rangle$ defines the uncorrelated shot-noise level. Variance $V_{\mathbf{k}_0,-\mathbf{k}_0}(t)<1$ implies squeezing of the relative number fluctuations below the shot-noise level. For the present case of the smallest momentum area, we refer to this as "raw" or unbinned squeezing.

For bosons the uncorrelated shot noise is determined by Poissonian statistics and we have

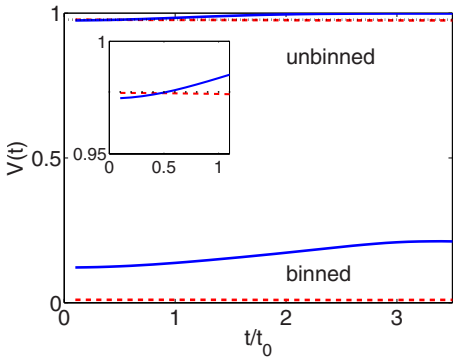

FIG. 4. (Color online) Relative number variance according to Eqs. (5) and (12), raw (unbinned) and binned, for fermions (solid blue) and bosons (dashed red). The dotted (black) line in the inset is the $t\ll t_0$ asymptote, Eq. (11). It is almost on top of the dashed line.

$$\Delta_{\mathrm{SN}}=\langle(\Delta\hat{n}_{1,\mathbf{k}_0})^2\rangle+\langle(\Delta\hat{n}_{2,-\mathbf{k}_0})^2\rangle=\langle\hat{n}_{1,\mathbf{k}_0}\rangle+\langle\hat{n}_{2,-\mathbf{k}_0}\rangle. \tag{6}$$

For fermions, on the other hand, the shot noise is always sub-Poissonian and is given by [28]

$$\begin{aligned}\Delta_{\mathrm{SN}}&=\langle(\Delta\hat{n}_{1,\mathbf{k}_0})^2\rangle+\langle(\Delta\hat{n}_{2,-\mathbf{k}_0})^2\rangle\\&=\langle\hat{n}_{1,\mathbf{k}_0}\rangle(1-\langle\hat{n}_{1,\mathbf{k}_0}\rangle)+\langle\hat{n}_{2,-\mathbf{k}_0}\rangle(1-\langle\hat{n}_{2,-\mathbf{k}_0}\rangle).\end{aligned} \tag{7}$$

The relative number variance can be written in the following form [10,19,29]:

$$V_{\mathbf{k}_0,-\mathbf{k}_0}(t)=\frac{\langle\hat{n}_{1,\mathbf{k}_0}\hat{n}_{1,\mathbf{k}_0}\rangle-\langle\hat{n}_{1,\mathbf{k}_0}\hat{n}_{2,-\mathbf{k}_0}\rangle}{\Delta_{\mathrm{SN}}}, \tag{8}$$

where we have taken into account that $\langle\hat{n}_{1,\mathbf{k}_0}\rangle=\langle\hat{n}_{2,-\mathbf{k}_0}\rangle\equiv n_{\mathbf{k}_0}$ and $\langle\hat{n}_{1,\mathbf{k}_0}\hat{n}_{1,\mathbf{k}_0}\rangle=\langle\hat{n}_{2,-\mathbf{k}_0}\hat{n}_{2,-\mathbf{k}_0}\rangle$. Note that $\langle\hat{n}_{1,\mathbf{k}_0}\hat{n}_{1,\mathbf{k}_0}\rangle=\langle\hat{n}_{1,\mathbf{k}_0}\rangle=n_{\mathbf{k}_0}$ for fermions. Applying Wick's theorem to calculate the higher-order moments and introducing the resonant anomalous density $m_{\mathbf{k}_0}\equiv\langle\hat{a}_{1,\mathbf{k}_0}\hat{a}_{2,-\mathbf{k}_0}\rangle$, where $\hat{a}_{j,\mathbf{k}}(t)\equiv\hat{a}_j(\mathbf{k},t)\sqrt{\Delta k_x\Delta k_y}$, we obtain

$$V_{\mathbf{k}_0,-\mathbf{k}_0}(t)=1-\frac{|m_{\mathbf{k}_0}|^2-n_{\mathbf{k}_0}^2}{n_{\mathbf{k}_0}} \tag{9}$$

for bosons and

$$V_{\mathbf{k}_0,-\mathbf{k}_0}(t)=1-\frac{|m_{\mathbf{k}_0}|^2}{n_{\mathbf{k}_0}(1-n_{\mathbf{k}_0})} \tag{10}$$

for fermions.

The variance $V_{\mathbf{k}_0,-\mathbf{k}_0}(t)$ can now be calculated by numerically solving Eq. (4) as before. The results are shown in Fig. 4 (upper curves), where we see a relatively small degree of squeezing for the present "raw" (unbinned) case.

We note that the unbinned squeezing for bosons and fermions has a common short-time asymptote that can be determined analytically using a perturbative approach [29]. Applying it to our 2D system gives

$$V_{\mathbf{k}_0,-\mathbf{k}_0} = 1 - 2R_{\mathrm{TF},x}R_{\mathrm{TF},y}\Delta k_x \Delta k_y/(9\pi) \simeq 0.978, \quad (11)$$

which agrees with our numerical results (see Fig. 4 inset).

The squeezing in the relative number can be enhanced for larger counting areas, which we refer to as binning [10]. We choose differently oriented bins for the bosons and fermions to reflect the difference in the direction of the anisotropy of the respective density distributions. For pairs of bins coinciding with the left (L) and right (R) halves of the momentum space for bosons and with the bottom (B) and top (T) halves for fermions, we can introduce particle number operators $\hat{N}_i^{L(R)}$ and $\hat{N}_i^{B(T)}$ ($i=1,2$). The normalized variance of the relative number fluctuations between the spin states 1 and 2 is defined similarly to Eq. (5),

$$V_{LR(BT)}(t) = \langle [\Delta(\hat{N}_1^{R(T)} - \hat{N}_2^{L(B)})]^2 \rangle / \Delta_{\mathrm{SN}}. \quad (12)$$

More explicitly, the particle number operators $\hat{N}_j^{L(R)}$ and $\hat{N}_j^{B(T)}$ ($j=1,2$) are defined as $\hat{N}_j^L = \Sigma^L \hat{n}_{j,\mathbf{k}}$ (with a similar convention for R, B, and T), where Σ^L and Σ^R stand for double sums $\Sigma^L \equiv \Sigma_{k_x<0}\Sigma_{k_y}$ and $\Sigma^R \equiv \Sigma_{k_x>0}\Sigma_{k_y}$, whereas $\Sigma^B \equiv \Sigma_{k_x}\Sigma_{k_y<0}$ and $\Sigma^T \equiv \Sigma_{k_x}\Sigma_{k_y>0}$.

In Eq. (12), the uncorrelated shot-noise level

$$\Delta_{\mathrm{SN}} = \sum^R \langle (\Delta \hat{n}_{1,\mathbf{k}})^2 \rangle + \sum^L \langle (\Delta \hat{n}_{2,\mathbf{k}})^2 \rangle \quad (13)$$

for bosons is given by

$$\Delta_{\mathrm{SN}} = \sum^R \langle \hat{n}_{1,\mathbf{k}} \rangle + \sum^L \langle \hat{n}_{2,\mathbf{k}} \rangle = \langle \hat{N}_1^R \rangle + \langle \hat{N}_2^L \rangle, \quad (14)$$

while for fermions it is given by

$$\Delta_{\mathrm{SN}} = \sum^T \langle \hat{n}_{1,\mathbf{k}} \rangle (1 - \langle \hat{n}_{1,\mathbf{k}} \rangle) + \sum^B \langle \hat{n}_{2,\mathbf{k}} \rangle (1 - \langle \hat{n}_{2,\mathbf{k}} \rangle), \quad (15)$$

which we note is not the same as $[\langle \hat{N}_1^T \rangle (1 - \langle \hat{N}_1^T \rangle) + \langle \hat{N}_2^B \rangle (1 - \langle \hat{N}_2^B \rangle)]$. Applying Wick's theorem to factorize the higher-order moments in Eq. (12) we obtain

$$V_{LR}(t) = \frac{1}{\langle \hat{N}_1^R \rangle} \Big[\langle \hat{N}_1^R \rangle + \sum_{\mathbf{k}}^R \sum_{\mathbf{k}'}^R |\langle \hat{a}_{1,\mathbf{k}}^\dagger \hat{a}_{1,\mathbf{k}'} \rangle|^2 - \sum_{\mathbf{k}}^R \sum_{\mathbf{k}'}^L |\langle \hat{a}_{1,\mathbf{k}} \hat{a}_{2,\mathbf{k}'} \rangle|^2 \Big] \quad (16)$$

for bosons and

$$V_{BT}(t) = \frac{1}{\langle \hat{N}_1^T \rangle - \sum_{\mathbf{k}}^T \langle \hat{n}_{1,\mathbf{k}} \rangle^2} \Big[\langle \hat{N}_1^T \rangle - \sum_{\mathbf{k}}^T \sum_{\mathbf{k}'}^T |\langle \hat{a}_{1,\mathbf{k}}^\dagger \hat{a}_{1,\mathbf{k}'} \rangle|^2 - \sum_{\mathbf{k}}^T \sum_{\mathbf{k}'}^B |\langle \hat{a}_{1,\mathbf{k}} \hat{a}_{2,\mathbf{k}'} \rangle|^2 \Big] \quad (17)$$

for fermions. Here, we have used the fact that $\langle \hat{n}_{1,\mathbf{k}} \rangle = \langle \hat{n}_{1,-\mathbf{k}} \rangle = \langle \hat{n}_{2,\mathbf{k}} \rangle$, $\langle \hat{N}_1^R \rangle = \langle \hat{N}_2^L \rangle$, and $\langle \hat{N}_1^T \rangle = \langle \hat{N}_2^B \rangle$ due to symmetry considerations.

The calculation of the variances $V_{LR}(t)$ and $V_{BT}(t)$ can now be done using the numerical solution of Eq. (4); the results are shown in Fig. 4 (lower curves). Comparing the upper and lower curves, we see that binning into momentum half spaces reduces the relative number variance, or increases the degree of squeezing, by a factor of about 10 for fermions and 100 for bosons. The difference in the fermionic and bosonic binned squeezings is due to the different momentum uncertainties of the source molecular BEC along the long and short spatial axes. The momentum uncertainty is about 10 times smaller along the long axis, which is the bosonic enhancement direction. Hence there are about 10 times less correlated pairs ending up in the same momentum half space. For the fermions, on the other hand, the relatively high-momentum uncertainty in the direction of higher atomic density produces more pairs in the same half space, reducing the number difference squeezing.

IV. SUMMARY

In summary, we have shown that dissociation of elongated condensates of molecular dimers into atoms can produce qualitatively different geometrical distributions for bosonic and fermionic atoms. The squeezing of the relative atom number fluctuations between half spaces can be quite strong.

Even though we have considered a two-dimensional system, we expect our results to be at least qualitatively valid for three-dimensional systems. For example, considering the dissociation of a 3D cigar-shaped molecular condensate with cylindrical symmetry along x (trap frequencies $\omega_x \ll \omega_y = \omega_z$), we expect that the results shown in Fig. 1 will be qualitatively similar to the cross sections of the full 3D distribution. For bosonic atoms this will imply enhanced emission in the opposite directions along x similar to 2D, while for fermions such cross sections will correspond to a toroidal 3D distribution pinned by the molecular condensate through the axis of symmetry. An interesting application of this geometry would be the generation of topologically nontrivial structures in two component Fermi gases. By similar geometric considerations, one could produce 3D enhanced emission of fermionic atoms propagating in opposite directions along x if the initial molecular condensate was prepared in a pancake trap with $\omega_x \gg \omega_y = \omega_z$. Analysis of these 3D geometries is currently underway.

ACKNOWLEDGMENTS

The authors acknowledge support from the Australian Research Council through the ARC Centre of Excellence scheme. M.Ö. acknowledges IPRS/UQILAS.

[1] T. Jeltes, J. M. McNamara, W. Hogervorst, W. Vassen, V. Krachmalnicoff, M. Schellekens, A. Perrin, H. Chang, D. Boiron, A. Aspect, and C. I. Westbrook, Nature (London) **445**, 402 (2007).
[2] M. Greiner, C. A. Regal, J. T. Stewart, and D. S. Jin, Phys. Rev. Lett. **94**, 110401 (2005).
[3] A. Perrin, H. Chang, V. Krachmalnicoff, M. Schellekens, D. Boiron, A. Aspect, and C. I. Westbrook, Phys. Rev. Lett. **99**, 150405 (2007).
[4] H. Pu and P. Meystre, Phys. Rev. Lett. **85**, 3987 (2000); A. Sørensen, L. –M. Duan, J. I. Cirac, and P. Zoller, Nature (London) **409**, 63 (2001).
[5] V. A. Yurovsky, Phys. Rev. A **65**, 033605 (2002).
[6] K. V. Kheruntsyan and P. D. Drummond, Phys. Rev. A **66**, 031602(R) (2002).
[7] A. Vardi and M. G. Moore, Phys. Rev. Lett. **89**, 090403 (2002).
[8] K. V. Kheruntsyan, M. K. Olsen, and P. D. Drummond, Phys. Rev. Lett. **95**, 150405 (2005).
[9] B. Zhao, Z. B. Chen, J. W. Pan, J. Schmiedmayer, A. Recati, G. E. Astrakharchik, and T. Calarco, Phys. Rev. A **75**, 042312 (2007).
[10] C. M. Savage and K. V. Kheruntsyan, Phys. Rev. Lett. **99**, 220404 (2007).
[11] A. Perrin, C. M. Savage, D. Boiron, V. Krachmalnicoff, C. I. Westbrook, and K. V. Kheruntsyan, New J. Phys. **10**, 045021 (2008).
[12] S. Inouye, A. P. Chikkatur, D. M. Stamper-Kurn, J. Stenger, D. E. Pritchard, and W. Ketterle, Science **285**, 571 (1999).
[13] M. Kozuma, Y. Suzuki, Y. Torii, T. Sugiura, T. Kuga, E. W. Hagley, and L. Deng, , Science **286**, 2309 (1999).
[14] M. G. Moore and P. Meystre, Phys. Rev. Lett. **83**, 5202 (1999).
[15] H. Uys and P. Meystre, Phys. Rev. A **77**, 063614 (2008).
[16] K. V. Kheruntsyan and P. D. Drummond, Phys. Rev. A **58**, R2676 (1998); Phys. Rev. A **61**, 063816 (2000).
[17] M. J. Davis, S. J. Thwaite, M. K. Olsen, and K. V. Kheruntsyan, Phys. Rev. A **77**, 023617 (2008).
[18] M. W. Jack and H. Pu, Phys. Rev. A **72**, 063625 (2005).
[19] C. M. Savage, P. E. Schwenn, and K. V. Kheruntsyan, Phys. Rev. A **74**, 033620 (2006).
[20] J. F. Corney and P. D. Drummond, Phys. Rev. Lett. **93**, 260401 (2004); Phys. Rev. B **73**, 125112 (2006).
[21] P. D. Drummond, K. V. Kheruntsyan, and H. He, Phys. Rev. Lett. **81**, 3055 (1998); D. J. Heinzen, R. Wynar, P. D. Drummond, and K. V. Kheruntsyan, *ibid.* **84**, 5029 (2000).
[22] E. Timmermans, P. Tommasini, M. Hussein, and A. Kerman, Phys. Rep. **315**, 199 (1999); J. Javanainen and M. Mackie, Phys. Rev. A **59**, R3186 (1999).
[23] S. J. J. M. F. Kokkelmans, J. N. Milstein, M. L. Chiofalo, R. Walser, and M. J. Holland, Phys. Rev. A **65**, 053617 (2002).
[24] P. D. Drummond and K. V. Kheruntsyan, Phys. Rev. A **70**, 033609 (2004).
[25] R. A. Duine and H. T. C. Stoof, Phys. Rep. **396**, 115 (2004); T. Köhler, K. Góral, and P. S. Julienne, Rev. Mod. Phys. **78**, 1311 (2006).
[26] For a given atom-molecule scattering length, the respective *s*-wave interaction energy per particle can be made negligible by operating at much higher absolute values of the dissociation detuning $|\Delta|$. This would, however, imply a higher velocity of the atoms, which may leave the molecular condensate region well before the atomic mode population reaches one and the difference between bosonic and fermionic statistics starts to show up. To surpass this problem one would need to use species with stronger values of the dissociation coupling χ in order to speed up the conversion and see the effects discussed here. While physically not impossible, this parameter regime would require a much larger computational lattice which is currently not feasible with our numerical method.
[27] For these values of $R_{\mathrm{TF},i}=(2U_{22}^{(2\mathrm{D})}\rho_{M,0}/m_2\omega_i^2)^{1/2}$ $(i=x,y)$, we have assumed the trap oscillation frequencies of $\omega_x/2\pi=2$ Hz and $\omega_y/2\pi=20$ Hz and used $\rho_{M,0}=3.2\times10^{12}$ m^{-2} as the 2D peak density of the molecular BEC. The effective 2D molecule-molecule interaction strength, $U_{22}^{(2\mathrm{D})}=U_{22}^{(3\mathrm{D})}/(\sqrt{2\pi}l_{2,z})$, where $U_{22}^{(3\mathrm{D})}=4\pi\hbar^2a_{22}/m_2$, a_{22} is the 3D molecule-molecule scattering length, and $l_{2,z}=\sqrt{\hbar/m_2\omega_z}$ is the length of the harmonic-oscillator ground state for the molecules in the eliminated z direction, is evaluated assuming $\omega_z/2\pi=500$ Hz and $a_{22}=1.4$ nm.
[28] K. V. Kheruntsyan, Phys. Rev. Lett. **96**, 110401 (2006).
[29] M. Ögren and K. V. Kheruntsyan, Phys. Rev. A **78**, 011602(R) (2008).